Time scales of tunneling decay of a localized state

Yue Ban,[1] E. Ya. Sherman,[1,2] J. G. Muga,[1] and M. Büttiker[3]
[1]*Department of Physical Chemistry, Universidad del País Vasco UPV-EHU, E-48080 Bilbao, Spain*
[2]*IKERBASQUE, Basque Foundation for Science, E-48011 Bilbao, Spain*
[3]*Département de Physique Théorique, Université de Genéve, CH-1211 Genéve 4, Switzerland*
(Received 18 August 2010; revised manuscript received 27 October 2010; published 30 December 2010)

Motivated by recent time-domain experiments on ultrafast atom ionization, we analyze the transients and time scales that characterize, aside from the relatively long lifetime, the decay of a localized state by tunneling. While the tunneling starts immediately, some time is required for the outgoing flux to develop. This short-term behavior depends strongly on the initial state. For the initial state, tightly localized so that the initial transients are dominated by over-the-barrier motion, the time scale for flux propagation through the barrier is close to the Büttiker-Landauer traversal time. Then a quasistationary, slow-decay process follows, which sets ideal conditions for observing diffraction in time at longer times and distances. To define operationally a tunneling time at the barrier edge, we extrapolate backward the propagation of the wave packet that escaped from the potential. This extrapolated time is considerably longer than the time scale of the flux and density buildup at the barrier edge.

DOI: 10.1103/PhysRevA.82.062121 PACS number(s): 03.65.Xp, 03.65.Nk, 03.75.−b

I. INTRODUCTION

Tunneling, being one of the most fundamental concepts in quantum mechanics, remains a source of strong theoretical and experimental controversy with regard to the relevant time scales of the process [1,2]. A typical tunneling setting is the scattering process, where a wave packet is reflected from and transmitted through a barrier higher than the incident particle energy. In this case the group delay [3], defined in terms of the energy derivatives of the reflection or transmission phase shift, is indicative of the motion of the wave-packet peak. It was also found that the group delay for particles tunneling through an opaque barrier is independent of the barrier width (the "Hartman effect" [4]).

Measurement of the time spent by a tunneling particle in the classically forbidden region can be based on the approach of Baz and Rybachenko [5,6], which uses the Larmor precession of a particle with a magnetic moment in a weak magnetic field or in effective fields in solids due to spin-orbit coupling [7,8]. In classically forbidden regions there is not only precession but also a rotation [9] of the moment into the direction of the field. Büttiker and Landauer [10] analyzed tunneling through an oscillating rectangular barrier and found an interaction time that is closely related to the rotation of the magnetic moment in a magnetic field [9,10]. A tunneling time has been measured for electromagnetic waves passing through inhomogeneous optical structures [11,12] and waveguides [13,14]. Interestingly, in graphene, a single layer of carbon atoms (which provides another example of massless particles), the transport occurs via evanescent waves, and the Wigner-Smith delay is *linear* in the tunneling distance [15].

Brouard *et al.*, using scattering-theory projectors for to-be-transmitted or reflected wave-packet parts and for localizing the particle at the barrier, set a formal framework that unified many of the existing proposals, pointing out that the multiple time scales correspond to different quantizations of the classical transmission time due to the noncommuting observables and possible orderings involved [16]. This clarified the meaning of different partitions of the dwell time into transmitted, reflected, and interference components. Another research line has been the investigation of characteristic times for the transient dynamics of the wave function (for example, the forerunners) in a plethora of potential configurations and initial conditions using asymptotic methods [17–19]. For specially prepared states, in particular, for confined or semiconfined initial waves with a flat density, these transients show diffraction in time [19,20], that is, temporal oscillations reminiscent of spatial Fresnel diffraction by a sharp edge [20]. Also, analysis of the partial density of states [21] provides another approach to understanding the tunneling process.

An important tunneling-dependent phenomenon is the decay of a metastable system [22–25], related, e.g., to state ionization in optics and to the discharging of a capacitor in mesoscopic physics [26–32]. Compared to the full-scattering problem, the decay configuration, or "half-scattering" problem, has been frequently considered unproblematic because of the absence of the transmitted or reflected wave-packet splitting and the existence of a well-known characterization in terms of resonance lifetimes. In fact, one may still pose classical questions regarding the tunneling time similar to those in the scattering configuration, however, without obvious answers. A particle may wander in the trapping well for a while and then escape through the barrier. For such a history the lifetime would be a waiting time in the well plus a tunneling time. Can this quantity be defined and measured in a sensible way? The understanding can be based on the analysis of quantum interference among the Feynman paths [33] or on the consideration of the quantities defined by operational procedures, as presented in this paper.

In recent years the techniques of atom ionization by a strong laser field and attosecond probing of electron dynamics opened a new venue for experimental studies of tunneling times. The measurement of He atom ionization [34] holds the promise of observing the tunneling delay of electrons in real time. In the experiment access to the dynamics at the tunneling time scale is gained through extrapolation of long time measurement to shorter times by assuming that a particle that has escaped through an energetically forbidden region into a classical allowed region follows classical dynamic laws. By using these laws and scattering data, the moment of escape

from the tunneling region into the classical region is determined. A related experiment [35] measures the perpendicular distribution of the nascent quantum-mechanical momentum uncertainty of the initial state as it is revealed by tunneling.

The aim of this paper is to study the dynamics of the tunneling-induced decay of a localized state and to investigate to what extent we can extract information on the short-time behavior from the long-time dynamics. We introduce a simple quantum-mechanical model that simulates the experimental measurement of tunneling time and allows for opening and closing the barrier [34]. We calculate the probability density and flux to study the short-term dynamics near the barrier and the long-term dynamics far away from it. For an opaque barrier we observe a relatively short transient time scale where the tunneling is developed into a quasisteady decay process. The details of the initial state have an important impact on the transients. At large distances the flux and the density start to grow at long times, reach a peak, and then decrease by diffraction-in-time oscillations. We found that the tunneling time obtained by extrapolating the particle motion from the position of the remote detector to the right edge of the barrier is not directly related to the time scale of the outgoing flux buildup.

II. GENERAL DESCRIPTION OF TUNNELING AND MODEL POTENTIAL

To study the tunneling dynamics, we consider the potential $U(x,t)$, which is infinite at $x < 0$. At $t < 0$ the potential holds bound states with wave function $\varphi_j(x)$ and energy E_j; it changes at $t = 0$ to allow the tunneling, and it changes back at $t = t_0$ to its initial form. The entire time dependence is

$$U(x,t) = \begin{cases} U_1(x) & (t < 0 \text{ and } t > t_0), \\ U_2(x) & (0 < t < t_0). \end{cases} \tag{1}$$

The initial state $\Psi(x,t = 0)$ prepared at $t = 0$ begins to evolve at $t > 0$, and the probability of finding the electron inside the potential decreases. This is similar to the ionization of an atom by a strong laser field, which allows a valence electron to tunnel through the barrier. At the closing time t_0, the potential becomes $U_1(x)$ again and the decay terminates. In the time interval $0 < t < t_0$ the wave function $\Psi(x,t)$ can be expressed as

$$\Psi(x,0 < t < t_0) = \int_0^\infty G(k)\phi_k(x) \exp\left(-\frac{ik^2 t}{2}\right) dk, \tag{2}$$

with

$$G(k) = \int_0^\infty \Psi(x,0)\phi_k(x)\, dx, \tag{3}$$

where $\phi_k(x)$ are delocalized real states in the potential $U_2(x)$ with the energy $E = k^2/2$. Here we use $\hbar \equiv m \equiv 1$ units, where m is the electron mass.

After closing the barrier at $t = t_0$, the potential gets its original form and the wave function can be expressed as

$$\Psi(x,t > t_0) = \sum_j B_j \varphi_j(x) \exp[-iE_j(t - t_0)] + \int_{\sqrt{2U_0}}^\infty B(k)\varphi_k(x) \exp\left[-\frac{ik^2(t - t_0)}{2}\right] dk, \tag{4}$$

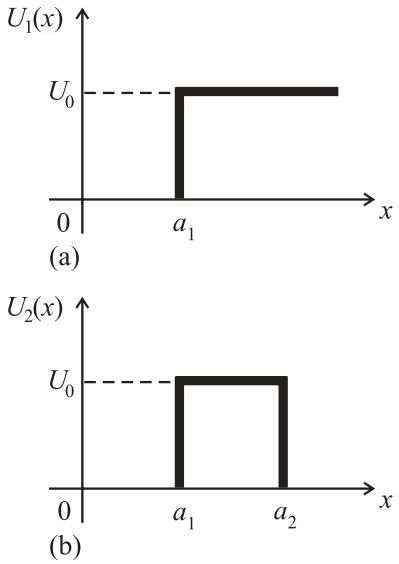

FIG. 1. The time-dependent potential $U_1(x)$ at $t = 0$ and $t > t_0$ and $U_2(x)$ within the interval $0 < t < t_0$. (a) $U_1(x)$ is a step in the positive half-plane, which is 0 from $x = 0$ to $x = a_1$ and U_0 from $x = a_1$ to infinity, while (b) presents a barrier that extends from $x = a_1$ to $x = a_2$ and is of the height of U_0. The potential is always infinite in the negative half-plane.

where summation is extended over the bound states of the initial potential, and

$$B_j = \int_0^\infty \Psi(x,t_0)\varphi_j(x)\, dx, \tag{5}$$

$$B(k) = \int_0^\infty \Psi(x,t_0)\varphi_k(x)\, dx, \tag{6}$$

with $\varphi_k(x)$ being the continuum states in the potential $U_1(x)$. With Eqs. (2) and (4) we have fully specified the time evolution of the escape problem.

To specify the model, we assume that at $t < 0$ the potential $U_1(x)$ is a step in the positive half-axis, being zero at $0 < x < a_1$ and U_0 at $x > a_1$, as shown in Fig. 1(a). At $t = 0$ the potential changes to $U_2(x)$, which is a rectangular barrier of the height U_0 extended from a_1 to a_2, as shown in Fig. 1(b). The rectangular barrier, being the simplest example of potential that is finite everywhere where the wave function and its derivative are continuous, allows for exact analysis of the dynamics. Here we set $a_1 \equiv 1$ and measure the time, energy, and momentum in the corresponding units.

The delocalized eigenstates of the Hamiltonian corresponding to $U_1(x)$ have the form

$$\varphi_k(x) = \begin{cases} C_1(k)\sin(kx) & (0 < x < a_1), \\ \sqrt{2/\pi}\,\sin[qx + \theta_1(k)] & (x > a_1), \end{cases} \tag{7}$$

where $q = \sqrt{k^2 - 2U_0}$ and $k > \sqrt{2U_0}$, with $C_1(k)$ and $\theta_1(k)$ determined by the boundary conditions at $x = a_1$, and the norm is determined by $\langle \varphi_{k'} | \varphi_k \rangle = \delta(q - q')$.

The eigenstate of the Hamiltonian corresponding to $U_2(x)$ is

$$\phi_k(x) = \begin{cases} C(k)\sin(kx) & (0 < x < a_1), \\ D(k)e^{-\kappa_k x} + F(k)e^{\kappa_k x} & (a_1 < x < a_2), \\ \sqrt{2/\pi}\,\sin[kx + \theta(k)] & (x > a_2), \end{cases} \quad (8)$$

with the normalization condition $\langle\phi_{k'}|\phi_k\rangle = \delta(k - k')$. The coefficients $C(k)$, $D(k)$, $F(k)$, and the phase $\theta(k)$ satisfy the boundary conditions of the potential $U_2(x)$, and $\kappa_k = \sqrt{2U_0 - k^2}$. In the tunneling regime $k < \sqrt{2U_0}$, while in the propagating regime $k > \sqrt{2U_0}$, and $i\kappa_k$ is substituted by q, defined previously.

III. TUNNELING DYNAMICS AT SHORT AND LONG TIMES

A. Decay of the state

The decay rate is described by the probability of finding the particle in the well from $x = 0$ to $x = a_1$, defined as

$$w_1(t) = \int_0^{a_1} \Psi^*(x,t)\Psi(x,t)\,dx. \quad (9)$$

The lifetime t_l, which also can be seen as the dwell time, an important time scale introduced to characterize the decay rate, is the time that it takes for the relative probability in the well $w_1(t)/w_1(0)$ to decay to $1/e$. For an opaque barrier the decay time can be written approximately as $t_l \approx AT_{k_0}\exp(2\kappa d)$, with $\kappa = \sqrt{2(U_0 - E_0)}$ and $d = a_2 - a_1$, where $k_0 = \sqrt{2E_0}$, $T_{k_0} = 2/k_0$ is the period of motion for a particle in the well, $\exp(-2\kappa d) \ll 1$ is the tunneling rate, and A is a barrier-dependent coefficient of order 1. Therefore, κd is a significant physical parameter with regard to the decay process and tunneling time. Analysis of different examples where this simple expression for the lifetime does hold can be found in Ref. [25].

To study the dynamics, we first set the initial state as the ground state of the Hamiltonian corresponding to $U_1(x)$ for a typical potential. For example, for $U_0 = 16$ there are two bound eigenstates: the ground $\varphi_0(x)$ (energy E_0) and the excited state $\varphi_1(x)$ (energy E_1). The energy E_0 for $\Psi(x,0) = \varphi_0(x)$ is 3.52. By choosing a different a_2, one can modify the transparency of the barrier. For example, if $\kappa d = 2$, corresponding to $a_2 = 1.4$, this barrier is moderately opaque. The corresponding $G(k)$ is shown in Fig. 2. Under the conditions of $\Psi(x,0) = \varphi_0(x)$, the lifetime in this potential is $t_l = 17.5$, as illustrated in Fig. 3(a). Calculated real and imaginary parts of $\Psi(x,t)$ after some short transients show fast oscillations with the envelope function $\exp(-t/2t_l)$. This behavior implies that in terms of the poles in the complex energy plane, the states we consider correspond to the simple Breit-Wigner resonances. Detailed analysis of various types of resonances and their relation to different time scales can be found in Refs. [36,37]. To clarify the influence of the initial state on tunneling, we alter it into the ground state of an infinite-wall potential, $\Psi(x,0) = \sqrt{2}\sin(\pi x)$. Therefore, E_0 is $\pi^2/2$ and a_2 becomes 1.42 to keep κd unchanged. As shown in Fig. 2, the coefficient $G(k)$ in Eq. (3) has two contributions related to the resonances corresponding to the bound states of the initial potential. For $\Psi(x,0) = \varphi_0(x)$, the second one, corresponding to the first excited state with a fast decay, is extremely weak. The presence of more than one bound state in the initial potential combined with the condition of low transparency of the barrier leads to important consequences for the short-time-scale tunneling dynamics.

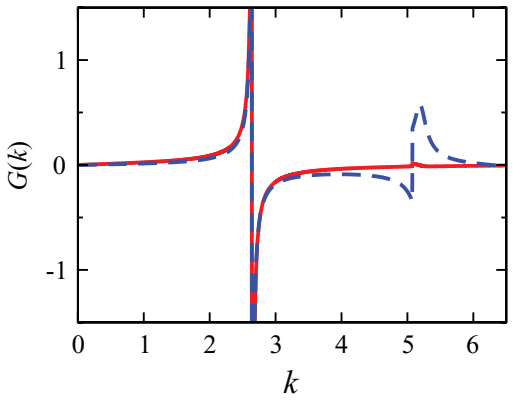

FIG. 2. (Color online) The matrix element $G(k)$ of the initial state with the delocalized states of the potential U_2, where k is the wave vector of the delocalized states. The solid line corresponds to the initial state $\Psi(x,0) = \varphi_0(x)$, which is a bound state of U_1. For this case the barrier in U_2 extends from $a_1 = 1$ to $a_2 = 1.4$. The dashed line corresponds to a sinusoidal initial state $\Psi(x,0) = \sqrt{2}\sin(\pi x)$ and to a barrier in U_2 extending from $a_1 = 1$ to $a_2 = 1.42$. In both cases, $\kappa d = 2$ and $U_0 = 16$.

Although all the probabilities decrease exponentially at long times, showing the general feature of the process, the ones with $\Psi(x,0) = \sqrt{2}\sin(\pi x)$ in Fig. 3(b) oscillate fast, while those with $\Psi(x,0) = \varphi_0(x)$ in Fig. 3(a) decay smoothly. This is because $\Psi(x,0) = \sqrt{2}\sin(\pi x)$ has a significant contribution of the second anomaly shown in Fig. 2, leading to interference with the "ground-state resonance."

B. Short-term dynamics

In this section we address the beginning of the tunneling by studying the short-time dynamics of the flux,

$$J(x,t) = \frac{1}{2i}\left[\Psi^*(x,t)\frac{\partial\Psi(x,t)}{\partial x} - \frac{\partial\Psi^*(x,t)}{\partial x}\Psi(x,t)\right], \quad (10)$$

and the density,

$$\rho(x,t) = \Psi^*(x,t)\Psi(x,t). \quad (11)$$

These two quantities satisfy the continuity equation,

$$\frac{\partial\rho(x,t)}{\partial t} + \frac{\partial J(x,t)}{\partial x} = 0. \quad (12)$$

Based on Eq. (12) we obtain the flux at the edges,

$$J(a_1,t) = -\frac{dw_1(t)}{dt}, \quad J(a_2,t) = \frac{dw_2(t)}{dt}, \quad (13)$$

where

$$w_2(t) = \int_{a_2}^{\infty} \Psi^*(x,t)\Psi(x,t)\,dx \quad (14)$$

is the probability of finding the particle outside the potential.

In Fig. 4 we illustrate the time dependence of the edge flux for different barriers during a short time scale for

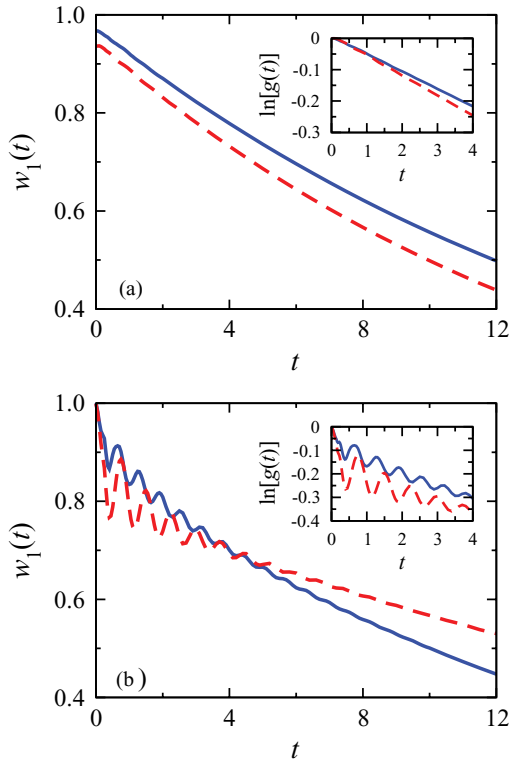

FIG. 3. (Color online) The probability of finding the particle in the well from 0 to a_1. (a) The solid and the dashed lines are for two initial states $\Psi(x,0) = \varphi_0(x)$, one for $U_0 = 16$ and the other for $U_0 = 10$. (b) The solid and the dashed lines represent the barriers $U_0 = 16$ and $U_0 = 10$, with the same initial state $\Psi(x,0) = \sqrt{2}\sin(\pi x)$. The insets exhibit $\ln[g(t)]$ at small time scale, where $g(t) \equiv w_1(t)/w_1(0)$. For all curves $\kappa d = 2$.

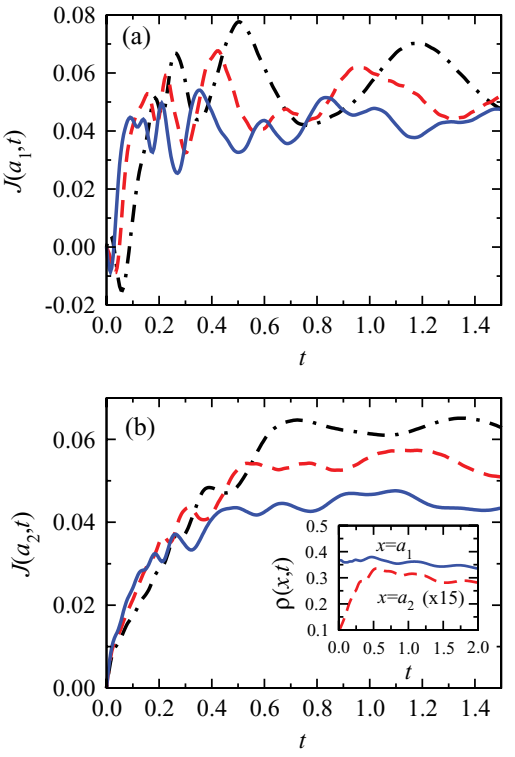

FIG. 4. (Color online) (a) Flux at the left edge a_1. The solid, dashed, and dot-dashed lines correspond to the barriers $U_0 = 24$, $U_0 = 16$, and $U_0 = 10$, respectively. (b) Flux at the right edge a_2. The inset presents the density at a_1 (solid) multiplied by 15 at a_2 (dashed), with the barrier $U_0 = 16$. All lines correspond to the same parameters as those in (a). For both plots, $\kappa d = 2$ and $\Psi(x,0) = \varphi_0(x)$.

$\Psi(x,0) = \varphi_0(x)$, where the lines shift to the right by lowering the barrier. It can be seen from both panels of Fig. 4 that $J(a_1,t)$ and $J(a_2,t)$ basically increase during a short time interval and then reach a rough plateau at a characteristic time $t_{\rm pl}$, which is a smoother behavior for $J(a_2,t)$, while $J(a_1,t)$ dives for a very short time to a negative value and oscillates more strongly. As a result, no feature can be clearly distinguished as a precise instant when tunneling begins. By using the continuity equations (13), the decay time t_l can be reliably estimated as $1/J_{\rm pl}(a_2)$, where $J_{\rm pl}(a_2)$ is the typical value of the flux at the plateau. The time scale when $J(a_2,t)$ develops a plateau also becomes larger, although it cannot be defined precisely. A crude estimate for the scale at which the plateau forms is $t_{\rm pl} \sim \pi/(2E_0)$, approximately a factor of 2 less than the oscillation period T_{k_0} of a particle in the initial well with potential U_1. The period T_{k_0} determines the prefactor of the escape time, as discussed previously with regard to Eq. (9). Therefore, classically speaking, the decay by tunneling as a steady process begins when the electron hits the barrier.

The inset in Fig. 4(b) shows the behavior of the density at the edge. In contrast to $J(a_1,0) = J(a_2,0) = 0$, $\rho(a_1,0)$ and $\rho(a_2,0)$ are not zero, as the ground state for the potential $U_1(x)$ is not fully localized in the well and the plateau in $\rho(a_2,0)$ is clearly seen.

Even though the numerically estimated times are much shorter, a similar trend in variation with the height of the barrier is shown by the Büttiker-Landauer time (BL time), provided that κd remains unchanged. The traversal time of Büttiker and Landauer [10], $t_{\rm BL} = d/\kappa$, given by the barrier width d divided by the "semiclassical" velocity $\kappa = [2(U_0 - E_0)]^{1/2}$, is an important time scale, especially in opaque conditions. With the conservation of κd, $t_{\rm BL}$ is proportional to $1/\kappa^2$.

The dependence of the flux at the right edge on time with different widths but keeping the height of the barrier is shown in Fig. 5(a). It is interesting that the time at which the flux begins to form a plateau is almost equal for the different widths, although the flux value at the plateau changes strongly, roughly as $\exp(-2\kappa d)$. In Fig. 5(b), this characteristic time $t_{\rm pl}$ also remains almost unchanged for different U_0 values by keeping the same width a_2. We conclude that the observed scale of $\pi/(2E_0)$ is universal and does not depend on the details of the potential.

For comparison, we illustrate in Fig. 6 the flux at a short time scale for a transparent barrier $\kappa d = 0.25$. As a matter of fact, the flux and the density have similar profiles. They grow from the initial to the maximum value and decrease rapidly, in contrast to the opaque behavior without an obvious peak. The peak is positioned at $t \approx 0.4$, similar to the time of plateau development in Fig. 5.

For the initial state $\Psi(x,0) = \sqrt{2}\sin(\pi x)$, the flux is enhanced by an order of magnitude and oscillates more strongly compared to the initial $\Psi(x,0) = \varphi_0(x)$, because $\sin(\pi x)$ contains larger contributions from different eigenstates. Different from that with $\Psi(x,0) = \varphi_0(x)$, the density

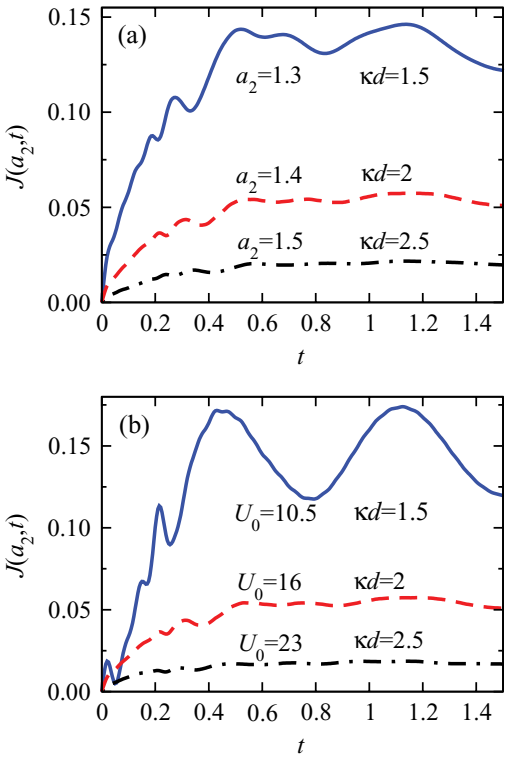

FIG. 5. (Color online) (a) Dependence of flux at the right edge on time with different widths: solid line, $\kappa d = 1.5$; dashed line, $\kappa d = 2$; and dot-dashed line, $\kappa d = 2.5$, $U_0 = 16$. (b) Dependence of flux at the right edge on time with different heights, by remaining $a_2 = 1.4$: solid line, $\kappa d = 1.5$; dashed line, $\kappa d = 2$; and dot-dashed line, $\kappa d = 2.5$, respectively. The ground-state energy E_0 depends only weakly on the potential height U_0. For all plots $\Psi(x,0) = \varphi_0(x)$.

is zero at $t = 0$ outside the barrier. The time dependence of the density at the edges with the initial state $\Psi(x,0) = \sqrt{2}\sin(\pi x)$ is presented in Fig. 7 for a typical barrier. For various system parameters, the delay time between the maximum of the density at the right and the left edges is in good agreement with the Büttiker-Landauer time $t_{\rm BL}$ for these potentials. We conclude that $t_{\rm BL}$ manifests itself as a delay time if

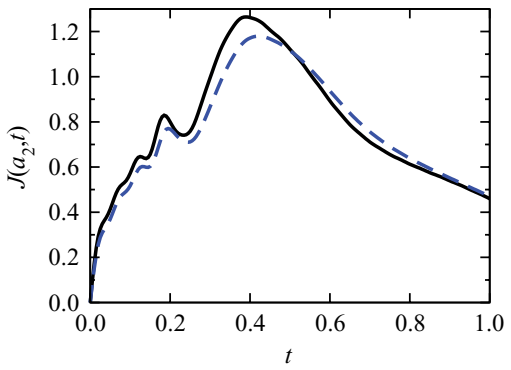

FIG. 6. (Color online) Time evolution of the flux at the right edge, where the solid line represents the flux when $U_0 = 16$ and $a_2 = 1.05$. The dashed line corresponds to the flux for $U_0 = 10$ and $a_2 = 1.06$. The two barriers are transparent as $\kappa d = 0.25$, and the initial state is $\varphi_0(x)$.

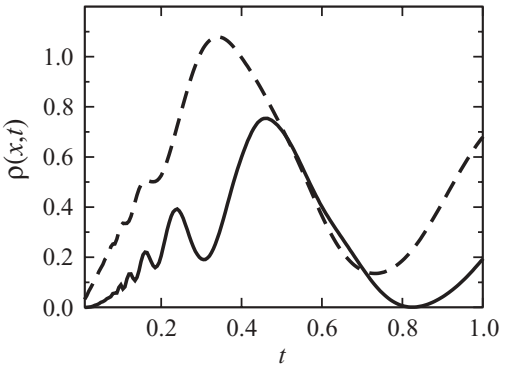

FIG. 7. Density evolution with the barriers $U_0 = 10$, $a_2 = 1.63$ (solid line at a_2 and dashed line at a_1). As the density at a_2 is relatively small, it is multiplied by the factor of 10. The barrier is opaque with $\kappa d = 2$, and the initial state is $\Psi(x,0) = \sqrt{2}\sin(\pi x)$.

over-the-barrier motion becomes essential due to the choice of the initial state. The momentum components that matter at first are the ones larger than $\sqrt{2U_0}$, as the momentum distribution of $\sin(\pi x)$ is broad. Moreover, its average local velocity at the right edge of the barrier $v_B(a_2,t) = J(a_2,t)/\rho(a_2,t)$ decreases from a large value with some oscillations to a relatively stable one close to $\sqrt{2E_0}$ during a short interval, after which the real tunneling starts. This means that the forerunners go just above the barrier instead of tunneling. By contrast, the tunneling process for $\Psi(x,0) = \varphi_0(x)$ occurs from the instant the decay initiates, because $v_B(a_2,t)$ is always smaller than $\sqrt{2U_0}$.

As discussed in [38,39] with analytical models, $t_{\rm BL}$ is a characteristic time describing different phenomena, among them over-the-barrier transients. This is rather paradoxical, given its association with "tunneling" in the defining formula, and it has surely not been fully appreciated. A more intuitive understanding of this unexpected role is still needed.

C. Long-term dynamics

We have now established that the short-time dynamics of the probability flux is governed by robust time scales. We next investigate the long-term dynamics with the goal of finding out whether a suitable extrapolation of the long-term scattering data can be used to gain information on the short-time dynamics. We find that after formation of steady tunneling, the particle probability density shows two distinct features. The first one is an almost uniform change in $\rho(x,t)$ for $x < a_1$, with $\rho(x,t) \approx \rho(x,0)\exp(-t/t_l)$. The second one can be viewed as a broad bump (wave packet) with relatively small density, propagating with the velocity close to $\sqrt{2E_0}$ and spreading in time. In this section we consider the dynamics of the bump at long time scales and trace it to short times to obtain the operationally defined tunneling times.

We assume that the flux $J(X,t)$ and the density $\rho(X,t)$ are measured by a detector located at $X \gg a_2$. It is shown in Fig. 8 for $\Psi(x,0) = \varphi_0(x)$ that the density at $X \gg a_2$ is nearly zero up to some time, then grows to a sharp maximum, and then decreases at time scales of t_l with the sequential oscillations due to the diffraction-in-time phenomenon [20]. The profiles of the flux and density are very similar, with $J(X,t) \approx \sqrt{2E_0}\rho(X,t)$.

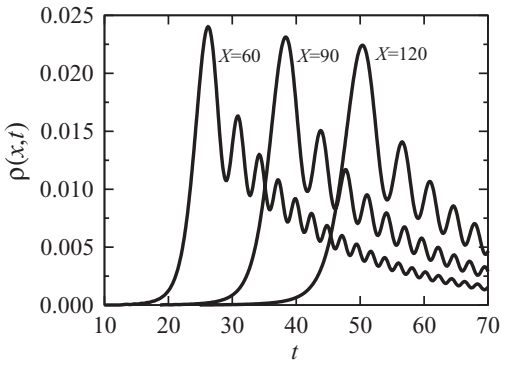

FIG. 8. Time evolution of density $\rho(X,t)$ at given positions $X = 60,90,120$, provided that $\Psi(x,0) = \varphi_0(x)$, $U_0 = 16$, $a_2 = 1.4$. A strong initial peak is followed by oscillations due to the diffraction-in-time process.

In the attosecond experiment analysis [34] the tunneling time was defined as the delay between the time when the barrier begins to be lowered and the time when the electron experiences acceleration by the external field, as can be extracted from the long-time behavior. Similarly, we can use the operational phenomenological approach to define a tunneling time as

$$t_{\mathrm{tun},1} = t_X - \frac{X - a_2}{\widetilde{v}_p}, \tag{15}$$

where t_X is the time when the detector measures the strongest first peak of the flux, $\widetilde{v}_p = \sqrt{2\widetilde{E}_0}$ is the velocity with which the particle moves out of the potential, and the energy

$$\widetilde{E}_0 = E_0 - \int_{a_2}^{\infty} U_0 \varphi_0^2(x)\, dx \tag{16}$$

is slightly less than E_0, as the potential changes suddenly from $U_1(x)$ to $U_2(x)$. As t_X is a measurable quantity, the tunneling time can be calculated by Eq. (15). For instance, for $\Psi(x,t = 0) = \varphi_0(x)$, $U_0 = 16$, $a_2 = 1.4$, when the detector is at $X = 120$, then $t_X = 50.3$, and the resulting $t_{\mathrm{tun},1} = 5.62$. Another approach, similar to Eq. (15), is to calculate the tunneling time as

$$t_{\mathrm{tun},2} = t_X - \frac{X - a_2}{v_X}, \tag{17}$$

where v_X is the velocity of the flux peak. For example, $v_X = 2.517$ as defined by the motion from $X = 120$ to $X = 122$. According to Eq. (17), the corresponding tunneling time is $t_{\mathrm{tun},2} = 3.18$. As it can be assumed that the velocity of the electron is constant outside the barrier in a classical manner, we can conclude that the tunneling time extracted from the measurements by a remote detector is X independent. Both Eqs. (15) and (17) extrapolate electron motion from the distance to the exit of the tunneling process. However, these two times are not equal either to the time of formation of the steady tunneling in Fig. 4 or to the decay time t_l.

Figure 9 depicts how the flux evolves with time and distance at two time scales for $\Psi(x,0) = \varphi_0(x)$. The curvature of the maximum flux region in Fig. 9(a) shows that it takes some time for the flux to develop a constant speed in free space. In addition, Fig. 9(a) demonstrates that a peak of the flux at a_2 appears at $t \approx 1$, smaller than $t_{\mathrm{tun},2}$ in Eq. (17).

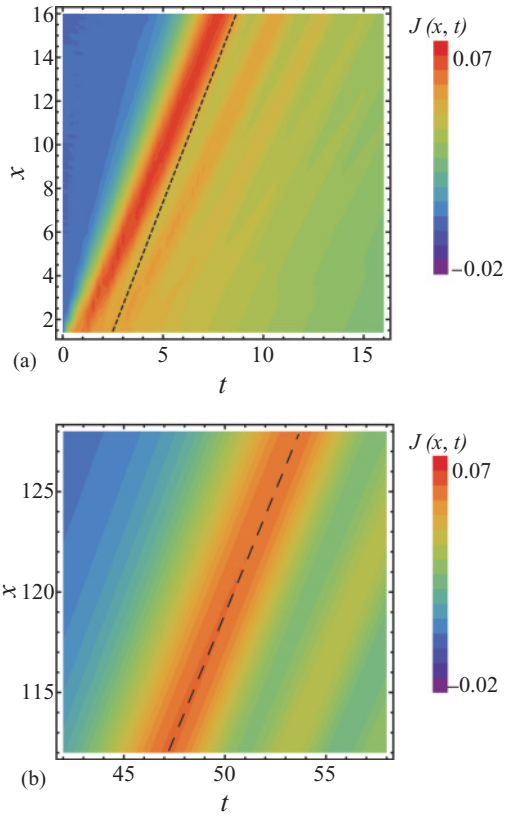

FIG. 9. (Color online) Flux vs time and position after a short time near the barrier (a) and after a long time far away from the barrier (b). All the parameters are the same as in Fig. 8. The dashed straight lines serve as a guide for the eye only. The short-dashed line in (a) demonstrates the nonlinearity of the peak position as a function of time. The long-dashed line in (b) shows that this dependence is very close to linear at those times and distances.

It is expected in some models that the wave function at long times and distances can be obtained with the stationary-phase approximation. Equation (2) in this limit can be recast as

$$\Psi(x > a_2,t) \approx \frac{1}{\sqrt{2\pi i}} \int_0^{\infty} dk\, G(k) \exp\left\{ i \left[\theta(k) + kx - \frac{k^2 t}{2} \right] \right\}, \tag{18}$$

and the phase $\theta(k) + kx - k^2 t/2$ can be expanded near the stationary point K, satisfying the equation $[d\theta(k)/dk]_{k=K} + x - Kt = 0$. However, $G(k)$ in our calculations is not a sufficiently smooth function near the K points due to the resonances shown in Fig. 2. Therefore, the stationary-phase approximation does not provide a satisfactory description of the peak propagation.

Another factor that affects the tunneling time is the closing time t_0, when the potential turns back from $U_2(x)$ to $U_1(x)$ and the tunneling is interrupted. The time evolution of the flux observed at the same remote position of the detector with different closing times is demonstrated in Fig. 10, and t_l is the exponential decay time introduced previously. The peak of the flux with shorter closing time t_0 appears earlier than that with longer t_0 as a result of the increased energy

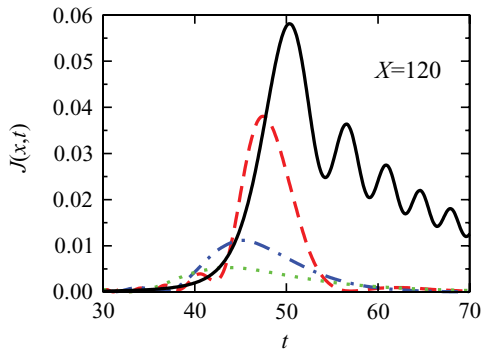

FIG. 10. (Color online) Flux as a function of time detected at $X = 120$ with different closing times: $t_0 = \infty$ (solid), $t_0 = t_l/3$ (dashed), $t_0 = t_l/6$ (dot-dashed), and $t_0 = t_l/9$ (dotted), where t_l is the lifetime for the particle in the case of $t_0 = \infty$. Other parameters are the same as those of Fig. 8.

spreading [40]. After the closing time t_0, the probability of finding the particle in the well remains almost unchanged. This shows that components with larger momenta tunnel through the barrier first and, therefore, closing the barrier can decrease the operationally defined times $t_{\mathrm{tun},1}$ and $t_{\mathrm{tun},2}$. Measurement of the total number of particles escaped from the potential as a function of closing time can help us to find the time scale of the flux formation t_{pl}. With the increase of t_0 through this region, the number of escaped particles, which is quadratic in t_0 for short times, changes at $t_0 > t_{\mathrm{pl}}$ to a linear dependence.

IV. CONCLUSIONS

Motivated by recent experiments on ultrafast atom ionization by optical fields, we have studied numerically and exactly, for a rectangular barrier, time-resolved tunneling for short time scales and further propagation at long times of an initially localized particle. The barrier we considered is opaque, but not extremely so, to ensure a reasonable tunneling probability. The probability-density evolution on a short time scale, much less than the decay time, depends strongly on the initial state. Depending on how this state is prepared, this short-term motion can include both under-the-barrier tunneling and over-the-barrier propagation, as seen in the evolution of the density and flux at the barrier edges. The tunneling starts instantly, however, some time of the order of $\pi/(2E_0)$, where E_0 is the ground-state energy in the initial potential and is required to develop the outgoing flux eventually proportional to the characteristic exponential decay rate $1/t_l$. As expected, there is a time delay between the flux development at the left and the right edges of the barrier. If the initial state is the ground state of the potential at $t < 0$, the time scale of the flux development is much longer than the Büttiker-Landauer traversal time expected for the given barrier parameters. However, if the initial state is more tightly localized, the Büttiker-Landauer time manifests itself as a time delay of the flux and density maxima between the left and right edges of the barrier.

At long times we have considered the propagation of the escaped wave packet at distances much larger than the scale of the potential. From the operational definition of the escape time, related to the position of the maximum of the wave-packet density, we have estimated the time the particles escaped from the potential. This time is also much longer than the traversal time for the given barrier. To determine the effect of the time dependence of the barrier, we implemented escape time windows considerably shorter than the tunneling decay time t_l. The increasing importance of faster components for shorter time windows leads to the extrapolated time estimated for closing potentials smaller than those of the potentials permanently open.

ACKNOWLEDGMENTS

E.Y.S. and J.G.M. are grateful for the support of University of Basque Country UPV-EHU (Grant No. GIU07/40), Basque Country Government (IT-472-10), and Ministry of Science and Innovation of Spain (FIS2009-12773-C02-01). M.B. is supported by the Swiss NSF, MaNEP, and the European ITN, NanoCTM.

[1] L. A. MacColl, Phys. Rev. **40**, 621 (1932).
[2] *Time in Quantum Mechanics*, edited by J. G. Muga, R. Sala Mayato, and I. L. Egusquiza (Springer, Berlin, 2002).
[3] E. P. Wigner, Phys. Rev. **98**, 145 (1955).
[4] T. E. Hartman, J. Appl. Phys. **33**, 3427 (1962).
[5] A. I. Baz, Sov. J. Nucl. Phys. **4**, 182 (1967); **5**, 161 (1967).
[6] V. F. Rybachenko, Sov. J. Nucl. Phys. **5**, 635 (1967).
[7] D. V. Khomitsky and E. Ya. Sherman, Europhys. Lett. **90**, 27010 (2010).
[8] B. Huang and I. Appelbaum, Phys. Rev. B **82**, 241202 (2010).
[9] M. Büttiker, Phys. Rev. B **27**, 6178 (1983).
[10] M. Büttiker and R. Landauer, Phys. Rev. Lett. **49**, 1739 (1982).
[11] A. M. Steinberg, P. G. Kwiat, and R. Y. Chiao, Phys. Rev. Lett. **71**, 708 (1993).
[12] Ch. Spielmann, R. Szipöcs, A. Stingl, and F. Krausz, Phys. Rev. Lett. **73**, 2308 (1994).
[13] A. M. Steinberg, Lect. Notes Phys. **734**, 333 (2008).
[14] D. Mugnai and A. Ranfagni, Lect. Notes Phys. **734**, 355 (2008).
[15] R. A. Sepkhanov, M. V. Medvedyeva, and C. W. J. Beenakker, Phys. Rev. B **80**, 245433 (2009).
[16] S. Brouard, R. Sala, and J. G. Muga, Phys. Rev. A **49**, 4312 (1994).
[17] S. Brouard and J. G. Muga, Phys. Rev. A **54**, 3055 (1996).
[18] M. Büttiker and H. Thomas, Ann. Phys. (Leipzig) **7**, 602 (1998).
[19] A. del Campo, G. García Calderón, and J. G. Muga, Phys. Rep. **476**, 1 (2009).
[20] M. Moshinsky, Phys. Rev. **88**, 625 (1952).
[21] V. Gasparian, T. Christen, and M. Büttiker, Phys. Rev. A **54**, 4022 (1996); M. Büttiker, Pramana J. Phys. **58**, 241 (2002).
[22] A. del Campo, F. Delgado, G. García-Calderón, J. G. Muga, and M. G. Raizen, Phys. Rev. A **74**, 013605 (2006).
[23] A. Marchewka and E. Granot, Phys. Rev. A **79**, 012106 (2009).

[24] G. Kälbermann, Phys. Rev. C **79**, 024613 (2009); **77**, 041601 (2008).
[25] N. G. Kelkar, H. M. Castañeda, and M. Nowakowski, Europhys. Lett. **85**, 20006 (2009).
[26] M. Büttiker, H. Thomas, and A. Pretre, Phys. Lett. A **180**, 364 (1993).
[27] J. Gabelli, G. Feve, J.-M. Berroir, B. Placais, A. Cavanna, B. Etienne, Y. Jin, and D. C. Glattli, Science **313**, 499 (2006).
[28] S. E. Nigg, R. Lopez, and M. Büttiker, Phys. Rev. Lett. **97**, 206804 (2006).
[29] G. Féve, A. Mahé, J.-M. Berroir, T. Kontos, B. Placais, D. C. Glattli, A. Cavanna, B. Etienne, and Y. Jin, Science **316**, 1169 (2007).
[30] M. Moskalets, P. Samuelsson, and M. Büttiker, Phys. Rev. Lett. **100**, 086601 (2008).
[31] J. Keeling, A. V. Shytov, and L. S. Levitov, Phys. Rev. Lett. **101**, 196404 (2008).
[32] M. Büttiker and M. Moskalets, Int. J. Mod. Phys. B **24**, 1555 (2010).
[33] D. Sokolovski, Lect. Notes Phys. **734**, 195 (2008).
[34] P. Eckle, A. N. Pfeiffer, C. Cirelli, A. Staudte, R. Döner, H. G. Muller, M. Büttiker, and U. Keller, Science **322**, 1525 (2008).
[35] L. Arissian, C. Smeenk, F. Turner, C. Trallero, A. V. Sokolov, D. M. Villeneuve, A. Staudte, and P. B. Corkum, Phys. Rev. Lett. **105**, 133002 (2010).
[36] N. G. Kelkar, M. Nowakowski, K. P. Khemchandani, and S. R. Jain, Nucl. Phys. A **730**, 121 (2004).
[37] N. G. Kelkar, K. P. Khemchandani, and B. K. Jain, J. Phys. G **32**, 1157 (2006).
[38] J. G. Muga and M. Büttiker, Phys. Rev. A **62**, 023808 (2000).
[39] F. Delgado, J. G. Muga, A. Ruschhaupt, G. García-Calderón, and J. Villavicencio, Phys. Rev. A **68**, 032101 (2003).
[40] A. del Campo, J. G. Muga, and M. Moshinsky, J. Phys. B **40**, 975 (2007).